https://doi.org/10.5194/egusphere-2026-5483
Preprint. Discussion started: 29 September 2026

Aerosol mixing state drives a supersaturation-dependent bias in cloud condensation nuclei hygroscopicity retrievals

Iarla Boyce[1] and Alice Cicirello[1]

[1]Centre for Climate Repair, University of Cambridge, Cambridge, UK

Correspondence: Iarla Boyce (ib541@cam.ac.uk)

Abstract. Cloud droplet number depends on aerosol hygroscopicity, the readiness of aerosol particles to take up water. Operational products retrieve this property, denoted κ, from cloud condensation nuclei (CCN) measurements and are widely used to constrain and evaluate models. The retrieval infers an activation threshold by matching cumulative particle number to measured CCN concentration, assuming that every particle above this diameter activates and none below it. This requires a hygroscopically uniform aerosol population. It is shown here that this assumption fails at a remote marine site, producing a systematic bias in retrieved κ. At the ARM Eastern North Atlantic site, retrieved κ falls from 0.28 to 0.06 across the measured supersaturation range, diverging from the value predicted by aerosol composition. A coincident hygroscopicity tandem differential mobility analyser record shows that genuine size-dependent hygroscopicity accounts for only about one-fifth of this decline and measures substantial hygroscopic heterogeneity. Forward-simulating the retrieval using the measured κ distributions reproduces the observations at every setpoint, accounting for 92–118 % of the discrepancy. Insufficiently hygroscopic particles fail to activate despite their size, causing the inferred activation diameter to be too large and biasing κ low through its inverse-cubic dependence on diameter. The observed supersaturation dependence is therefore largely a mixing-state-dependent retrieval artefact rather than an aerosol property. When propagated through an aerosol activation calculation, use of retrieved rather than predicted κ produces an approximately 9–20 % underestimate in predicted cloud droplet number. More generally, integration-based CCN retrievals can convert aerosol mixing-state heterogeneity into apparent supersaturation dependence, affecting observational constraints on aerosol activation and aerosol–cloud interactions.

1 Introduction

Operational products retrieve aerosol hygroscopicity (κ) from cloud condensation nuclei (CCN) measurements to constrain and evaluate climate models (Uin et al., 2019; Kulkarni et al., 2021). The physical composition of marine aerosol, particularly the balance between highly hygroscopic sulfate and less hygroscopic organics, can shift the supersaturation required for activation by a factor of two to three (Petters and Kreidenweis, 2007). While Dusek et al. (2006) showed that particle size generally matters more than these compositional shifts for CCN activity, retrieving κ accurately remains important. Because κ enters directly into the activation calculations that predict cloud droplet number (N_d) (Abdul-Razzak and Ghan, 2000), a systematic error in an operational product does not average out like natural variability. Instead, it biases the activation threshold across the entire size distribution, propagating directly into N_d.

https://doi.org/10.5194/egusphere-2026-5483
Preprint. Discussion started: 29 September 2026

The CCN counter operates at a fixed instrument supersaturation, referred to as a setpoint. At each setpoint S, a measured size distribution is integrated downward from its upper limit until the cumulative particle number matches the measured CCN concentration (Kulkarni et al., 2021). The diameter at which the two match is taken as the critical activation diameter D_c. κ is then obtained from D_c and S using κ-Köhler theory (Köhler, 1936; Petters and Kreidenweis, 2007). This procedure assumes activation is a sharp function of size. Every particle larger than D_c is assumed to activate, and every particle smaller than it is assumed not to. This assumption holds only for a chemically uniform population, meaning a chemically heterogeneous population can produce an artificial supersaturation dependence (Kulkarni et al., 2021). This assumption does not hold for remote marine aerosol, as sea salt, sulfate, and biogenic organics coexist and external mixing is common in this environment (Ovadnevaite et al., 2011; Zheng et al., 2018). Whether this real-world heterogeneity is severe enough to systematically bias an operational retrieval, and by how much, is the question addressed here.

Closure studies at ENA and comparable remote marine sites report agreement between retrieved and composition-predicted κ within calibration uncertainty (Zheng et al., 2018; Zawadowicz et al., 2021; Gallo et al., 2023), but at few supersaturations, meaning a supersaturation-dependent bias would not be visible. Size-resolved studies have characterised how κ varies with particle size within single campaigns (Bougiatioti et al., 2011; Cerully et al., 2011) without testing a retrieval against it. Xu et al. (2021) examined how simplified hygroscopicity and mixing-state assumptions affect closure at Mace Head, but derived hygroscopicity from sub-saturated growth factors rather than CCN activation, so the quantity tested was not the retrieved one. Most directly, Ai et al. (2026) report a supersaturation-dependent degradation of bulk CCN closure at this same site from aircraft measurements, and attribute it to size-dependent aerosol composition, using two supersaturation channels and a bulk closure-ratio metric, without an independent measurement of the mixing state. None of these studies could separate a genuine size dependence of κ from a supersaturation-dependent failure of the retrieval. Doing so requires three things at once: enough supersaturation setpoints to resolve a trend, an independent measurement of the population's mixing state, and a simulation of the retrieval itself. No previous study combined all three. The ARM Eastern North Atlantic site on Graciosa Island, Azores (Mather and Voyles, 2013), routinely samples five setpoints and operates a co-located HTDMA, meeting the first two requirements. The simulation is supplied here.

2 Data and methods

2.1 Site and measurement period

The ARM ENA site, Graciosa Island, Azores (39.09°N, 28.03°W, 30 m a.s.l.) (Mather and Voyles, 2013), sits in the remote North Atlantic marine boundary layer. It is dominated by clean, recirculating marine air under the Azores High in summer, and more frequently influenced by North American continental outflow in autumn and winter (Zheng et al., 2018). The period analysed is April–July 2023, covering the spring-to-summer transition. The ACSM record over this period shows a stable organic-to-sulfate mass ratio, with no systematic biomass-burning or dust signatures.

Two analysis windows are used and must be distinguished. The closure statistics use the full April–July 2023 record. The HTDMA comparison and the forward simulation are restricted to 1 April – 24 May 2023, because the ENA HTDMA ceased

https://doi.org/10.5194/egusphere-2026-5483
Preprint. Discussion started: 29 September 2026

operating after that date. Where CCN quantities are quoted for the shorter window they are labelled explicitly, since campaign medians differ modestly between the two.

2.2 SMPS-CCN retrieval and its algorithm

The primary dataset is the ARM SMPS-based CCN-κ product (Kulkarni and Uin, 2023), which retrieves κ at each supersaturation setpoint from a DMT CCN counter operated in series with a scanning mobility particle sizer (Kulkarni et al., 2021). The SMPS classifies particles by electrical mobility diameter and requires no refractive-index assumption. The product is ARM production-grade (VAP 1.2.0).

The retrieval integrates the measured $\mathrm{d}N/\mathrm{d}\log D_p$ downward from the upper size limit until the cumulative concentration matches the measured N_{CCN}, yielding D_c, from which

$$\kappa = \frac{4A^3}{27\,D_c^3\,\ln^2(1+S)}, \qquad A = \frac{4\sigma_w M_w}{R_g T \rho_w}, \tag{1}$$

with $\sigma_w = 0.072\,\mathrm{N\,m^{-1}}$ the pure-water surface tension, M_w the molar mass of water, ρ_w the density of water and R_g the gas constant. This algorithm is reimplemented in Sect. 2.5 and validated against the product's own reported D_c.

Quality control retains only records where the ARM flags for κ, critical diameter and supersaturation are all zero, and where both S and κ are positive and finite. Five setpoints are populated across the campaign, nominally $S = 0.07$, 0.16, 0.33, 0.66 and 0.83%, with median critical diameters of approximately 183, 142, 112, 74 and 67 nm.

2.3 ACSM composition and κ_{pred}

Composition is taken from the ARM aerosol chemical speciation monitor (Zawadowicz, 2023), which measures submicron non-refractory mass concentrations of sulfate, organics, nitrate and chloride (Ng et al., 2011). Its aerodynamic-lens transmission falls off outside an approximately 75–650 nm vacuum aerodynamic diameter window. Its collection efficiency is corrected using the standard composition-dependent CDCE method (Middlebrook et al., 2012; Shilling and Levin, 2021). That correction is itself a model-based adjustment, not a direct measurement. Both add uncertainty in how representative bulk $\mathrm{PM_1}$ composition is of the population activating at a given D_c. The composition-predicted hygroscopicity is

$$\kappa_{\mathrm{pred}} = \sum_i \frac{V_i}{V_{\mathrm{tot}}}\,\kappa_i, \tag{2}$$

with $V_i = M_i/\rho_i$ the volume fraction of species i. Species values are given in Table 1.

The campaign median is $\kappa_{\mathrm{pred}} = 0.283 \pm 0.009$ (day-block bootstrap standard error). Although organics dominate the submicron mass (organic-to-sulfate mass ratio ≈ 1.8), sulfate contributes $\approx 70\%$ of κ_{pred} because organic hygroscopicity is low. κ_{pred} is a model estimate, not an observational ground truth. It assumes internal mixing, size-independent bulk composition, and fixed literature κ_i and ρ_i.

$\delta\kappa$ is defined as $\kappa_{\mathrm{pred}} - \kappa_{\mathrm{obs}}$, so a positive $\delta\kappa$ indicates the activating particles behave as less hygroscopic than the bulk-composition average. Because κ_{org} is itself assumed, Table 2 reports the sensitivity of $\delta\kappa$ to it at $S = 0.16\%$.

https://doi.org/10.5194/egusphere-2026-5483
Preprint. Discussion started: 29 September 2026

Table 1. Species hygroscopicity parameters (Petters and Kreidenweis, 2007) and assumed bulk densities used in Eq. (2).

Species	κ_i	ρ_i (g cm^{-3})
Sulfate (SO_4)	0.61	1.70
Organics (org)	0.10	1.35
Nitrate (NO_3)	0.67	1.73
Chloride (Cl)	1.28	1.52

Table 2. Sensitivity of κ_{pred} and $\delta\kappa$ at $S = 0.16\%$ ($\kappa_{\mathrm{obs}} = 0.184$) to the assumed organic hygroscopicity.

κ_{org}	κ_{pred}	$\delta\kappa$
0.05	0.250	+0.066
0.10	0.283	+0.099
0.20	0.348	+0.164
0.30	0.415	+0.231

2.4 HTDMA sub-saturated hygroscopicity

An independent constraint is provided by the ARM HTDMA at ENA (Uin et al., 2021), which operated until 24 May 2023. The instrument selects a dry mobility diameter and measures the hygroscopic growth-factor distribution at sub-saturated relative humidity, from which a κ distribution is derived independently of any CCN activation measurement. Five dry diameters are sampled: 50, 100, 150, 200 and 250 nm. At each selected size, the HTDMA returns a distribution of κ, resolved into 60 bins weighted by particle number concentration, rather than a single value. That distribution allows the mixing-state assumption underlying the CCN retrieval to be tested directly.

The same quality control as the CCN product is applied, requiring the ARM flags for dry diameter setting, total concentration and DMA relative humidity all to be zero. After quality control 3578 scans over 52 days are retained. For each scan the number-weighted mean, median and standard deviation of κ, the interquartile range, the dispersion $\sigma_\kappa/\bar{\kappa}$, and the number fractions falling in three hygroscopicity bands are computed: nearly hydrophobic ($\kappa < 0.10$), less hygroscopic ($0.10 \le \kappa < 0.40$) and more hygroscopic ($\kappa \ge 0.40$). Resolved modes are counted in the lightly smoothed weighted distribution. A peak is counted if it exceeds 10% of the distribution's maximum, and is separated from a neighbouring peak by a dip below 60% of the smaller of the two. This mode count is a conservative proxy, not a formal test of multimodality.

For matching to the CCN retrieval, HTDMA scans are paired to CCN records within 45 minutes and interpolated between adjacent dry-diameter settings.

https://doi.org/10.5194/egusphere-2026-5483
Preprint. Discussion started: 29 September 2026

2.5 Forward simulation of the retrieval

The CCN retrieval is forward-simulated under the measured mixing state. The backward-integration algorithm is reimplemented independently, taking bin widths from the product's own reported diameter bounds and log-interpolating to find the crossing diameter within the bin where the cumulative count matches N_{CCN}. Applied to the product's own size distribution and N_{CCN}, this reimplementation reproduces the product's own reported D_c. This validates the algorithm before it is used.

The measured mixing state is represented as a κ probability distribution, built from the campaign number-weighted HTDMA data at each dry diameter, on a common grid spanning $0 \leq \kappa \leq 2$ and interpolated across $\log D$ between the five measured sizes. Outside 50–250 nm the nearest measured size is used. Concentration recorded at $\kappa < 0$, corresponding to a growth factor below unity, is folded into the lowest bin, since those particles do not activate.

For an internally mixed population, every particle is assigned a single reference value κ_{ref}. Activation at each record's own supersaturation S follows

$$\kappa_{\mathrm{crit}}(D, S) = \frac{4A^3}{27\,D^3 \ln^2(1+S)}. \tag{3}$$

The activated number is summed to a synthetic N_{CCN} and passed through the retrieval algorithm. Because activation is sharp in size by construction under a uniform-κ population, the algorithm recovers κ_{ref} to within a small residual, which reflects the discretisation of the simulation and bounds its accuracy.

For an externally mixed population, the single κ is replaced by the measured distribution, so the activated number in each size bin is $n(D)\,P(\kappa \geq \kappa_{\mathrm{crit}} \mid D)$. Summing over size gives a synthetic N_{CCN} that reflects the real mixing state, and the retrieval algorithm is applied to it as it would be to real data, yielding a simulated D_c and κ. The simulation is run separately for each of 5095 quality-controlled records, using that record's own size distribution and supersaturation, and the internally and externally mixed outputs are compared with κ_{obs}.

2.6 UHSAS-CCN product

A second CCN-κ product based on optical sizing by an ultra-high sensitivity aerosol spectrometer (Kulkarni et al., 2023) is used for methodological comparison only (Kulkarni et al., 2021). It is ARM evaluation-grade and has not been certified for standard scientific analysis. The UHSAS retrieves optical diameter assuming a single fixed refractive index. Marine organics have a lower real index ($n \approx 1.45$–1.50) than the sulfate-dominated composition assumed ($n \approx 1.52$–1.53), so a particle scatters less light than assumed at a given size and the inversion compensates with a smaller optical diameter (Cai et al., 2008; Kupc et al., 2018). This product is used to demonstrate the sensitivity of the retrieval to its size-distribution input.

2.7 Cloud droplet activation

To express the consequences for users of the product, N_d is computed from the two-mode Abdul-Razzak and Ghan (2000) scheme. For each mode j with dry geometric mean diameter $D_{g,j}$, number concentration N_j, geometric standard deviation

https://doi.org/10.5194/egusphere-2026-5483
Preprint. Discussion started: 29 September 2026

$\sigma_{g,j}$ and hygroscopicity κ_j, the modal critical supersaturation is

$$S_{c,j} = \sqrt{\frac{4A^3}{27\,\kappa_j D_{g,j}^3}}, \tag{4}$$

and peak supersaturation $S_{\max}$ is the fixed point of

$$\frac{1}{S_{\max}^2} = \sum_j \frac{1}{S_{c,j}^2}\left[f_j \left(\frac{\zeta}{\eta_j}\right)^{3/2} + h_j \left(\frac{S_{c,j}^2}{\eta_j + 3\zeta}\right)^{3/4} \right], \tag{5}$$

with $f_j = 0.5\exp(2.5\ln^2\sigma_{g,j})$, $h_j = 1 + 0.25\ln\sigma_{g,j}$, and ζ, η_j the standard updraft and condensation-sink terms (Abdul-Razzak and Ghan, 2000). Equation (5) is solved by fixed-point iteration from $S_{\max}^{(0)} = 0.15\%$, evaluating each mode's κ_j at the current $S_{\max}$ by interpolation of the measured $\kappa_{\rm obs}$–S relationship, until successive iterates differ by less than 10^{-8}. Activated fractions follow as

$$\phi_j = \tfrac{1}{2}\,\mathrm{erfc}\left(\frac{2\ln(S_{c,j}/S_{\max})}{3\sqrt{2}\ln\sigma_{g,j}}\right), \qquad N_d = \sum_j N_j\,\phi_j. \tag{6}$$

Surface tension is held at the pure-water value throughout, matching the assumption made by the retrieval itself, so that the comparison isolates the effect of the κ input rather than introducing a second difference.

Mode number concentrations are obtained by direct trapezoidal integration of the measured spectra over 15–90 nm (Aitken) and 90–500 nm (accumulation), giving campaign medians of 235 and 202 cm^{-3} respectively. Fitted lognormal shape parameters ($D_g = 45$ nm, $\sigma_g = 1.69$ Aitken; $D_g = 171$ nm, $\sigma_g = 1.41$ accumulation) are retained, but fitted amplitudes are not used, because the unbounded lognormal integral includes an analytic tail below the 15 nm fit cutoff that is not a real particle count.

2.8 Significance testing

Day-block bootstrap resampling ($n_{\rm boot} = 2000$, seed 42, resampling whole days) gives standard errors that are robust to within-day autocorrelation. A naive record-level bootstrap underestimates these by a factor of about three, because consecutive marine-aerosol observations are strongly correlated. All confidence intervals in this study use the day-block procedure.

Two systematic terms are additionally propagated for the closure discrepancy, both treated as constant-fractional and applied independently at each setpoint. The first is SMPS sizing uncertainty. Because $\kappa \propto D_c^{-3}$, a fractional D_c uncertainty ϵ_D propagates to $\delta\kappa/\kappa = 3\epsilon_D$. A conservative value of $\epsilon_D = 3\%$ is adopted. The second is supersaturation calibration uncertainty. Because $\kappa \propto S_c^{-2}$, this propagates to $\delta\kappa/\kappa = 2\epsilon_S$, and a value of $\epsilon_S = 5\%$ is adopted, following Rose et al. (2008). The full-budget z-score combines both systematic terms with the two bootstrap standard errors in quadrature. Both ϵ values are literature-typical rather than drawn from this instrument's own calibration history, which was not available.

https://doi.org/10.5194/egusphere-2026-5483
Preprint. Discussion started: 29 September 2026

3 Results

3.1 A supersaturation-resolved discrepancy

Figure 1 plots the retrieved κ_{obs} against the composition-predicted κ_{pred} at each setpoint, alongside the critical diameters those setpoints correspond to, and Table 3 gives the matching statistics over the full April–July 2023 record. The two agree at the largest-particle setpoint, where κ_{obs} is statistically indistinguishable from κ_{pred}, and separate monotonically as the critical diameter falls. Figure 2 tracks this separation directly, showing both the discrepancy and its significance growing smoothly toward smaller particles rather than jumping at any one setpoint. Sample sizes are comparable across setpoints, so this trend is not an artefact of uneven statistical weight.

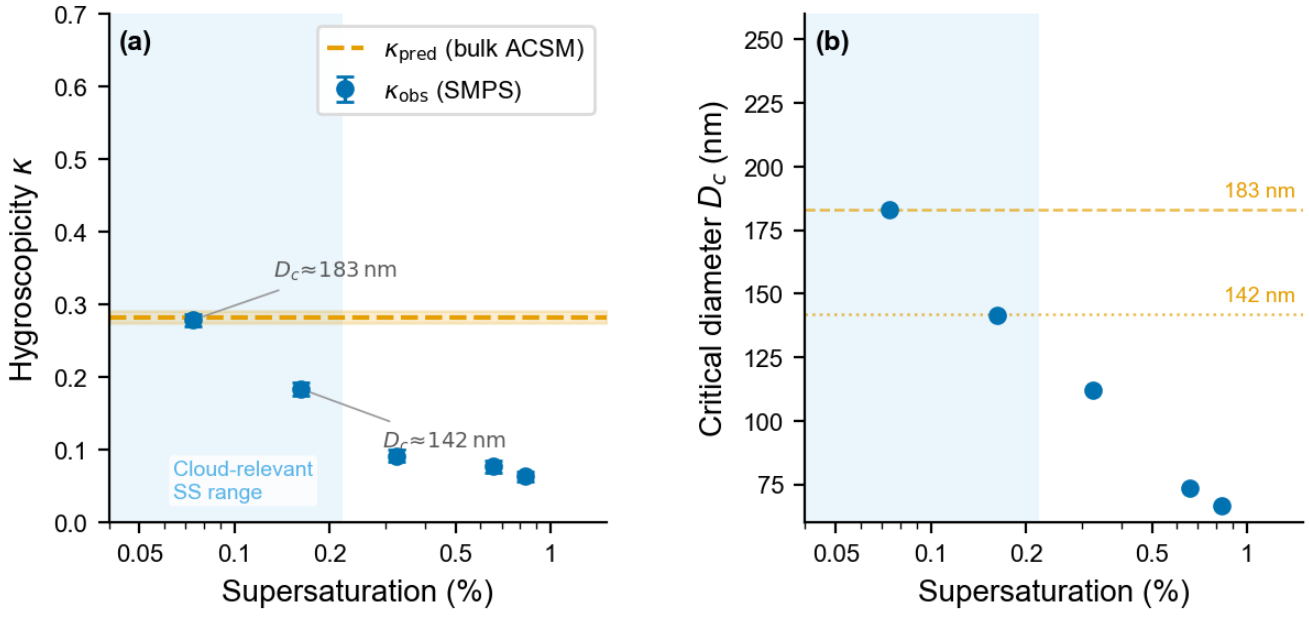

Figure 1. (a) CCN-retrieved κ_{obs} against supersaturation setpoint, April–July 2023. The horizontal line marks $\kappa_{\mathrm{pred}} = 0.283$ from bulk ACSM composition, with shading giving ± 1 day-block bootstrap standard error. κ_{obs} matches κ_{pred} at the lowest supersaturation ($D_c \approx 183$ nm) and declines monotonically thereafter. (b) The corresponding critical diameters. Shading marks the supersaturation range most relevant to marine stratocumulus.

A Mann-Kendall trend test on the five setpoint medians confirms a perfectly monotonic decrease ($\tau = -1.00$, $p = 0.017$, the minimum attainable for $n = 5$). A Benjamini-Hochberg correction at $\alpha = 0.05$ rejects the null at four of the five setpoints.

The systematic sizing and supersaturation errors that would be required to close this discrepancy are evaluated in Sect. 4.1.

https://doi.org/10.5194/egusphere-2026-5483
Preprint. Discussion started: 29 September 2026

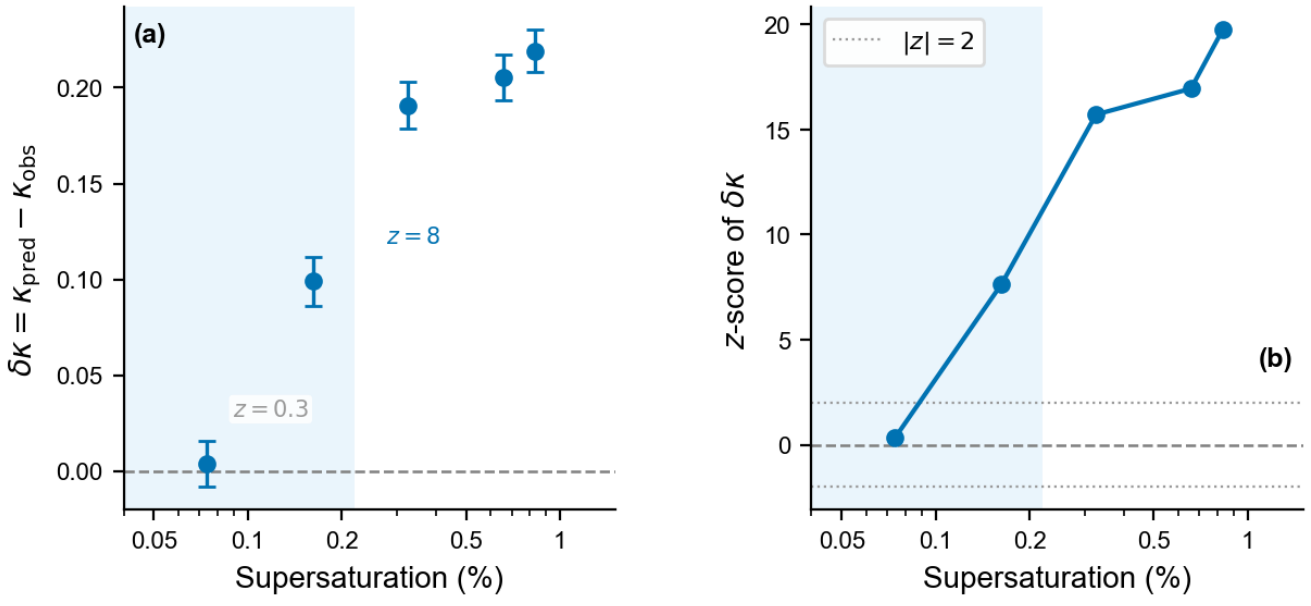

Figure 2. Significance of the closure discrepancy $\delta\kappa = \kappa_{\mathrm{pred}} - \kappa_{\mathrm{obs}}$ at each setpoint. (a) $\delta\kappa$ with ± 1 day-block bootstrap standard error. (b) $z = \delta\kappa / \mathrm{SE}_{\delta\kappa}$, with $|z| = 2$ marked. The discrepancy is indistinguishable from zero at $S \approx 0.07\%$ and highly significant at every higher setpoint.

Table 3. Per-setpoint closure statistics, April–July 2023. z_{boot} uses day-block bootstrap standard errors only; z_{full} additionally propagates the systematic budget of Sect. 2.8.

S (%)	D_c (nm)	n	κ_{obs}	$\delta\kappa$	z_{boot} / z_{full}
0.07	183	2240	0.279 ± 0.008	$+0.004$	0.3 / 0.1
0.16	142	2237	0.184 ± 0.009	$+0.099$	7.7 / 3.6
0.33	112	2231	0.092 ± 0.008	$+0.191$	15.5 / 10.9
0.66	74	2226	0.077 ± 0.008	$+0.206$	16.8 / 12.8
0.83	67	2224	0.064 ± 0.007	$+0.219$	19.5 / 15.5

https://doi.org/10.5194/egusphere-2026-5483
Preprint. Discussion started: 29 September 2026

3.2 An independent constraint from sub-saturated HTDMA

Table 4 reports the number-weighted HTDMA κ at each selected dry diameter. It rises with size from 0.331 at 50 nm to 0.479 at 250 nm, flattening above approximately 150 nm. Size-dependent hygroscopicity is therefore present at this site, in the same direction as the CCN retrieval implies.

Table 4. Number-weighted HTDMA κ by selected dry diameter, 1 April – 24 May 2023. Values are medians across scans of the per-scan number-weighted statistic.

D (nm)	n scans	peak bin	wt. median	wt. mean
50	688	0.308	0.331	0.386
100	919	0.391	0.388	0.439
150	996	0.422	0.422	0.472
200	605	0.420	0.447	0.508
250	370	0.441	0.479	0.655

The magnitudes, however, do not match. Table 5 pairs the HTDMA with each CCN setpoint on coincident air masses, interpolated to that setpoint's own critical diameter. Across the critical-diameter range (175 to 60 nm) the HTDMA κ declines by a factor of 1.29 while κ_{obs} declines by a factor of 3.63. In logarithmic terms the independent instrument reproduces approximately 20% of the retrieved decline.

Table 5. HTDMA κ matched to each CCN setpoint's critical diameter, coincident air masses, 1 April–24 May 2023. κ_{obs} here is the median over this shorter window and so differs from Table 3. The final column gives the ratio of HTDMA weighted-median κ to κ_{obs}.

S (%)	D_c (nm)	κ_{obs}	HTDMA wt. median	n matched	$\kappa_{\mathrm{HTDMA}}/\kappa_{\mathrm{obs}}$
0.07	175	0.316	0.442	356	1.40
0.16	134	0.218	0.424	441	1.95
0.33	105	0.110	0.402	405	3.64
0.66	67	0.103	0.369	356	3.59
0.83	60	0.087	0.342	308	3.92

Size-dependent composition is therefore real but insufficient. It cannot on its own account for the retrieved trend.

HTDMA κ is derived under sub-saturated conditions, and systematic differences from supersaturated behaviour are documented and expected (Swietlicki et al., 2008). The comparison is also restricted to the first 54 days of the study period.

https://doi.org/10.5194/egusphere-2026-5483
Preprint. Discussion started: 29 September 2026

3.3 The population is externally mixed at every size

The same HTDMA record tests the assumption underlying the retrieval directly. Table 6 and Fig. 3 report the width of the number-weighted κ distribution and the number fractions in three hygroscopicity bands.

Table 6. HTDMA mixing-state metrics by dry diameter, 1 April – 24 May 2023. Dispersion is $\sigma_\kappa/\bar{\kappa}$; normalised IQR is the interquartile range divided by the median; the final column is the fraction of scans resolving two or more modes.

D (nm)	dispersion	norm. IQR	$\kappa < 0.10$	$\kappa \geq 0.40$	multimodal
50	0.826	1.182	0.139	0.405	47.4%
100	0.727	0.922	0.086	0.455	47.2%
150	0.655	0.865	0.054	0.541	37.4%
200	0.684	0.934	0.052	0.578	47.6%
250	0.770	1.120	0.085	0.606	71.1%

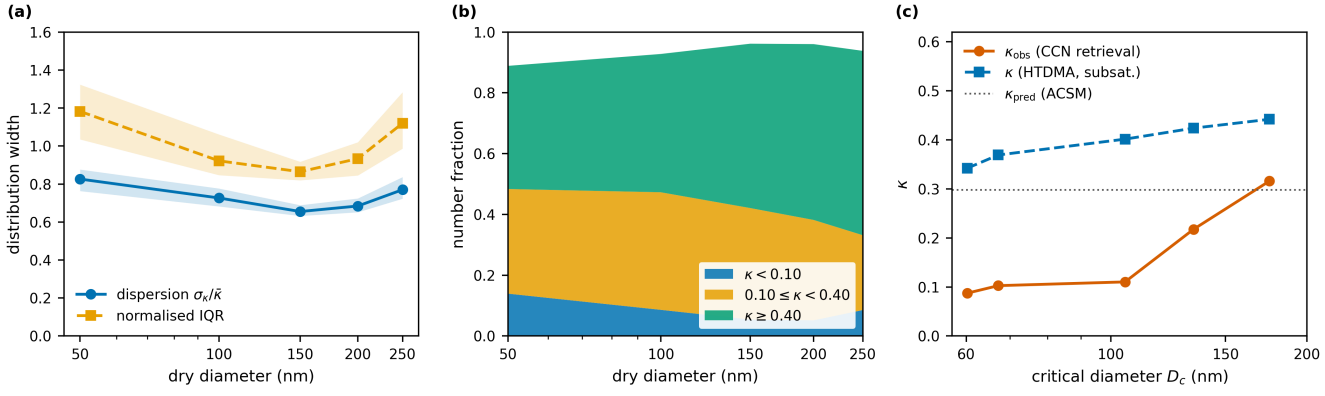

Figure 3. (a) Width of the number-weighted HTDMA κ distribution against dry diameter, as dispersion $\sigma_\kappa/\bar{\kappa}$ and normalised interquartile range. Shading gives day-block bootstrap 95% intervals. (b) Number fractions in three hygroscopicity bands. (c) CCN-retrieved κ_{obs} and sub-saturated HTDMA κ against critical diameter, with κ_{pred} marked.

The dispersion is 0.66–0.83 at every size sampled, and the normalised interquartile range is comparable to the median itself. Between 37% and 71% of scans resolve two or more modes. This is not a chemically uniform population at any size, and the uniformity assumption underlying the retrieval is therefore not satisfied at this site. The width does not increase monotonically toward smaller particles. It is lowest at 150 nm and rises at both ends. The fraction of strongly hygroscopic particles ($\kappa \geq 0.40$) falls monotonically with size, from 0.606 at 250 nm to 0.405 at 50 nm. This fraction matters more to the retrieval than the width of the distribution does. At a given supersaturation, it sets how many particles of that size are hygroscopic enough to activate, and how many are not.

https://doi.org/10.5194/egusphere-2026-5483
Preprint. Discussion started: 29 September 2026

3.4 Forward simulation reproduces the discrepancy

Reimplementing the retrieval algorithm and applying it to the product's own $\mathrm{d}N/\mathrm{d}\log D_p$ and N_{CCN} reproduces the product's own reported D_c to a median of $+0.01$ nm (interquartile range -0.12 to $+0.18$ nm) across 5095 records. The internally-mixed control recovers the input $\kappa_{\mathrm{ref}} = 0.421$ to a ratio of 0.943 (interquartile range 0.927–0.966). That 6% residual is a discretisation artefact of the finite bin grid, equivalent to about 2% in D_c, and bounds the accuracy of what follows.

A synthetic N_{CCN} is computed from the measured κ distributions and passed through the retrieval algorithm, and the resulting κ tracks κ_{obs} closely at all five setpoints, accounting for 92–118% of the discrepancy relative to the internally-mixed reference (Table 7). Figure 4a plots the simulated and observed κ together against supersaturation, alongside the internally-mixed reference, showing the simulated curve falling away from that reference in step with the real data rather than merely landing near it at each point. Figure 4b makes the match explicit, plotting the fraction of the discrepancy the simulation accounts for at each setpoint directly.

Table 7. Forward simulation against observation, 1 April – 24 May 2023, 5095 records. κ_{ref} is the internally-mixed reference. The explained fraction is $(1-\kappa_{\mathrm{sim}}/\kappa_{\mathrm{ref}})/(1-\kappa_{\mathrm{obs}}/\kappa_{\mathrm{ref}})$.

S (%)	κ_{ref}	κ_{sim}	κ_{obs}	explained
0.07	0.421	0.324	0.316	92.1%
0.16	0.421	0.181	0.218	118.1%
0.33	0.421	0.116	0.110	98.1%
0.66	0.421	0.112	0.103	97.1%
0.83	0.421	0.105	0.087	94.7%

Under external mixing, a substantial fraction of large particles are insufficiently hygroscopic to activate at the applied supersaturation. Figure 5a shows this schematically, fewer particles activate than the size-sharp assumption predicts, so the measured N_{CCN} is smaller than that assumption implies. Figure 5b traces the consequence for the retrieval itself. Because the backward integration only stops once the cumulative count reaches this smaller N_{CCN}, it terminates at too large a diameter. This inflated diameter produces a large deficit in retrieved κ from only a modest error in D_c, as $\kappa \propto D_c^{-3}$. The non-activating fraction grows as D_c falls, so the bias grows with supersaturation. The forward simulation reproduces both the magnitude and the shape of this trend.

3.5 Corroborating signatures in the CCN data alone

Two features of the CCN record itself are consistent with the mechanism, independent of the HTDMA. Figure 6a shows the activated fraction $N_{\mathrm{CCN}}/N_{\mathrm{tot}}$ rising with supersaturation, but saturating near 0.5 at the highest setpoints rather than approaching unity as the critical diameter falls into the Aitken mode. Figure 6b shows the fraction of quality-controlled records returning $\kappa_{\mathrm{obs}} < 0.10$, which rises from 1.4% at the lowest setpoint to 67% at the highest. Values below 0.10 imply a nearly hydrophobic

https://doi.org/10.5194/egusphere-2026-5483
Preprint. Discussion started: 29 September 2026

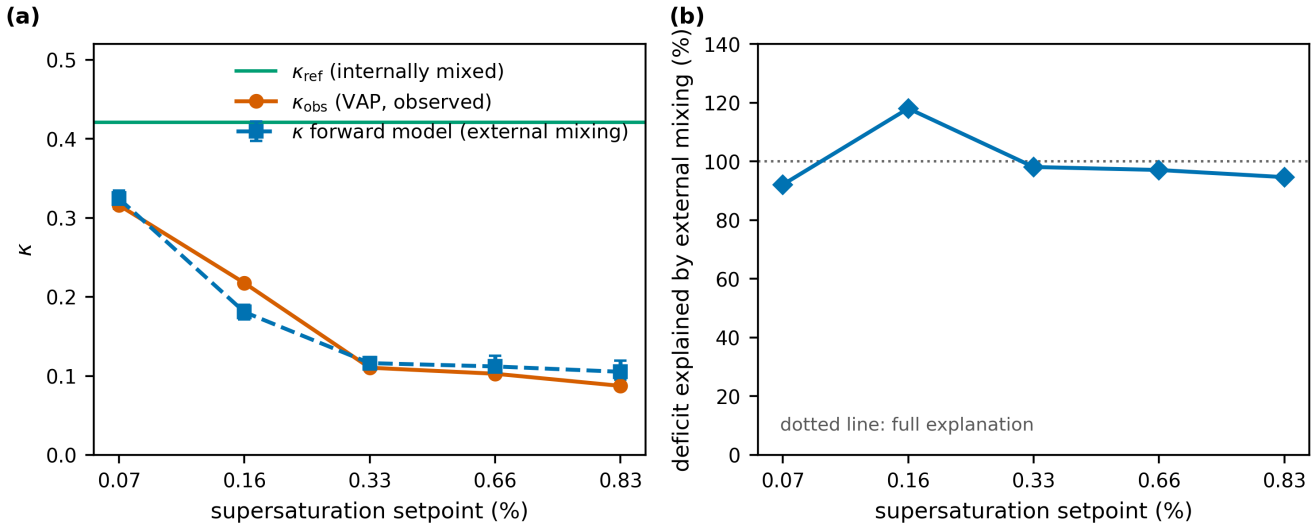

Figure 4. (a) Simulated and observed κ against supersaturation setpoint, with the internally-mixed reference marked. Error bars are day-block bootstrap 95% intervals on the simulation. (b) Fraction of the observed discrepancy accounted for by external mixing alone.

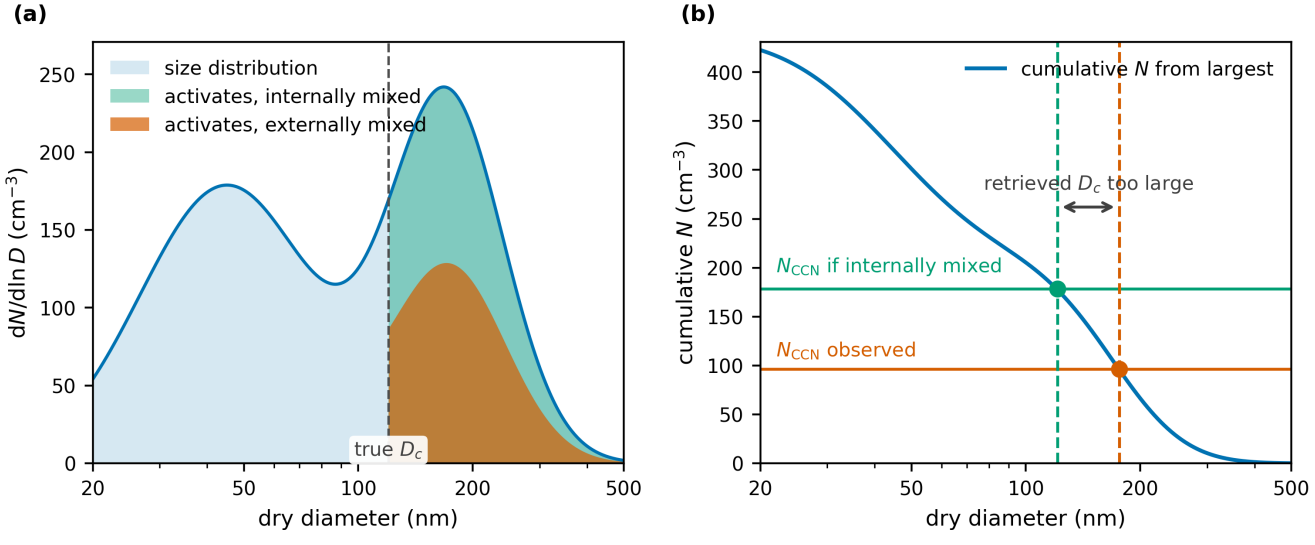

Figure 5. Why external mixing biases an integration-based κ retrieval. (a) For an internally mixed population every particle above the true critical diameter activates. For an externally mixed population only the sufficiently hygroscopic fraction does, so fewer particles activate at the same supersaturation. (b) The retrieval integrates the size distribution downward from the largest particles until the cumulative number matches the measured CCN concentration. The lower CCN concentration produced by external mixing is reached at a larger diameter, so the retrieved D_c exceeds the true value and κ, which varies as D_c^{-3}, is underestimated. Representative values are used for illustration.

https://doi.org/10.5194/egusphere-2026-5483
Preprint. Discussion started: 29 September 2026

aerosol, implausible at this site. At the three highest setpoints ($S = 0.33$, 0.66 and 0.83%), these low-κ records make up a large fraction of the retained sample, a majority at two of them. At $S = 0.07\%$ and $S = 0.16\%$, the corresponding fractions are 1.4% and 17%. As D_c falls, the non-activating fraction grows, and the retrieved κ moves toward implausible values.

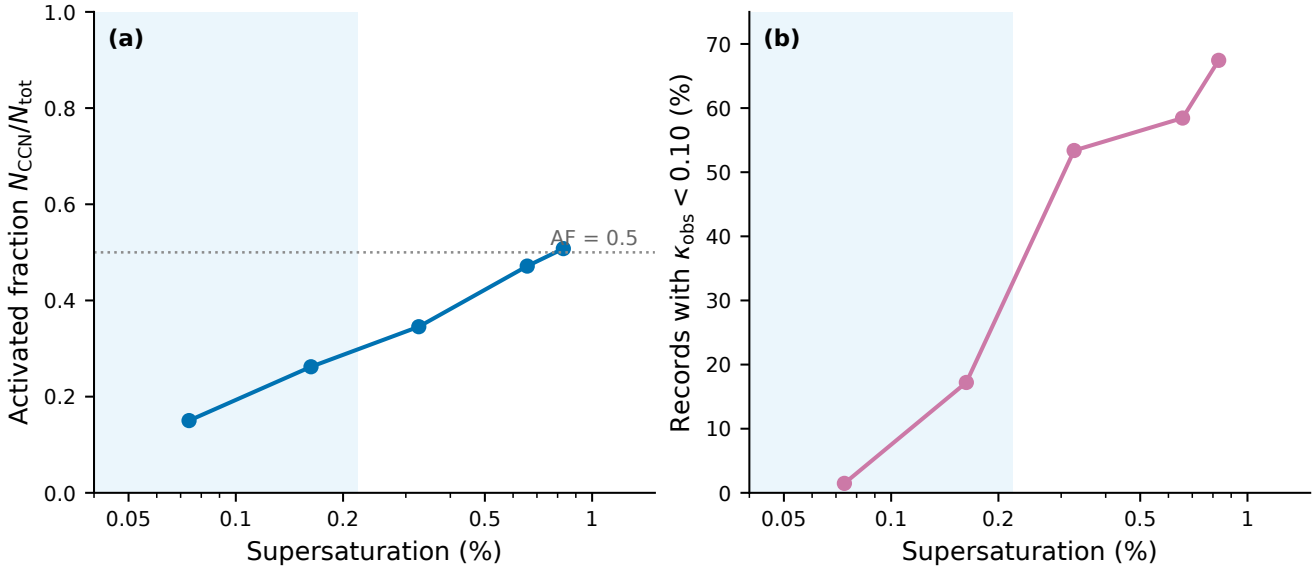

Figure 6. (a) Median activated fraction $N_{\mathrm{CCN}}/N_{\mathrm{tot}}$ at each supersaturation setpoint; the dotted line marks 0.5 for reference. (b) Percentage of quality-controlled records with $\kappa_{\mathrm{obs}} < 0.10$. Blue shading marks the supersaturation range most relevant to marine stratocumulus.

3.6 Sensitivity to the size-distribution input

An independent demonstration of the retrieval's sensitivity to its size input comes from the UHSAS-based product. A bin-by-bin comparison of coincident UHSAS and SMPS spectra ($n = 2859$ hours) shows a systematic UHSAS undercount across most of the 80–350 nm range. Figure 7 plots this undercount against particle diameter. It is deep and roughly constant at 23–24% from 80–142 nm, then partially recovers to 8–13% near 200–220 nm.

At the setpoint where the SMPS product gives $\kappa_{\mathrm{obs}} = 0.184$, the UHSAS product gives approximately 0.357. Figure 8 shows this reversal directly. The UHSAS value exceeds κ_{pred}, flipping the sign of the discrepancy rather than reducing it.

Because $\kappa \propto D_c^{-3}$, this UHSAS κ implies an effective critical diameter of approximately 114 nm, a 20% reduction from the SMPS value. That reduction agrees, in order of magnitude, with the 23% particle-number undercount shown in Fig. 7.

3.7 The sign of the N_d bias

Using the lower retrieved κ_{obs} in place of the reference κ reduces predicted N_d. Table 8 quantifies this underestimate across updraft velocity and loading. It grows from 9–12% at $w = 0.1\,\mathrm{m\,s^{-1}}$ to 15–20% at $w = 0.5\,\mathrm{m\,s^{-1}}$, and is consistently a little

https://doi.org/10.5194/egusphere-2026-5483
Preprint. Discussion started: 29 September 2026

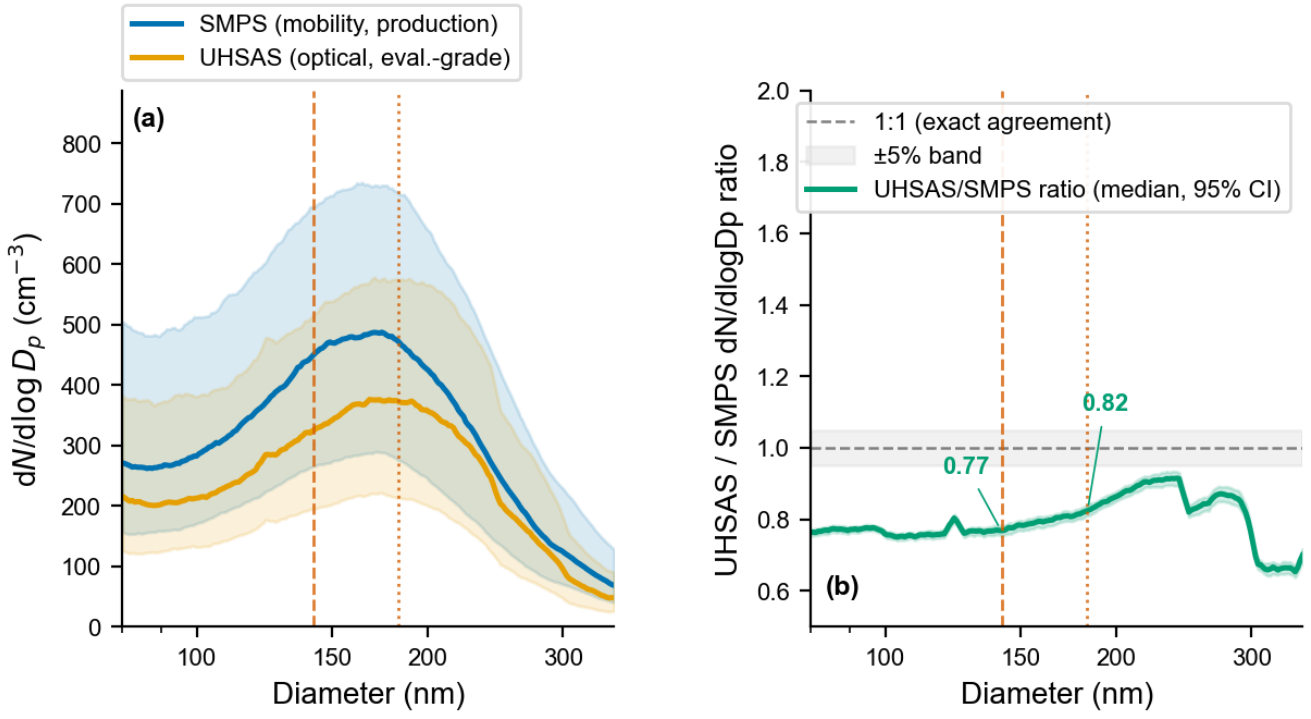

Figure 7. UHSAS-to-SMPS ratio of $\mathrm{d}N/\mathrm{d}\log D_p$ against particle diameter, coincident hours only ($n = 2859$). Vertical lines mark $D_c \approx 142$ nm and $D_c \approx 183$ nm.

larger under clean loading ($N_{\mathrm{acc}} \approx 120\,\mathrm{cm}^{-3}$) than typical loading ($N_{\mathrm{acc}} \approx 200\,\mathrm{cm}^{-3}$) at the same updraft velocity. Figure 9 extends this comparison over the full (w, N_{acc}) parameter space.

Repeating the calculation for every quality-controlled hourly spectrum ($n = 11{,}070$ hours across 122 days) at $w = 0.2\,\mathrm{m\,s}^{-1}$ gives a median N_d difference of 13.9%, with the same sign in every hour and every day. Using a shape-resolved accumulation mode rather than the campaign-median shape gives 8.7%.

Propagating a 15% N_d difference through the Twomey susceptibility $\partial A/\partial \ln N_d = A(1-A)/3$ (Platnick and Twomey, 1994) at a representative marine stratocumulus albedo gives an albedo difference of order 0.01.

4 Discussion

4.1 Ruling out alternative explanations

A systematic sizing bias could produce this trend but closing the discrepancy at $S = 0.16\%$ through sizing error alone would require a D_c bias of 19 nm, or 13.4%. A bias of this size is well beyond the calibration accuracy expected of a mobility particle sizer (Wiedensohler et al., 2012). Closing the discrepancy through supersaturation error alone requires $\Delta S/S$ of

https://doi.org/10.5194/egusphere-2026-5483
Preprint. Discussion started: 29 September 2026

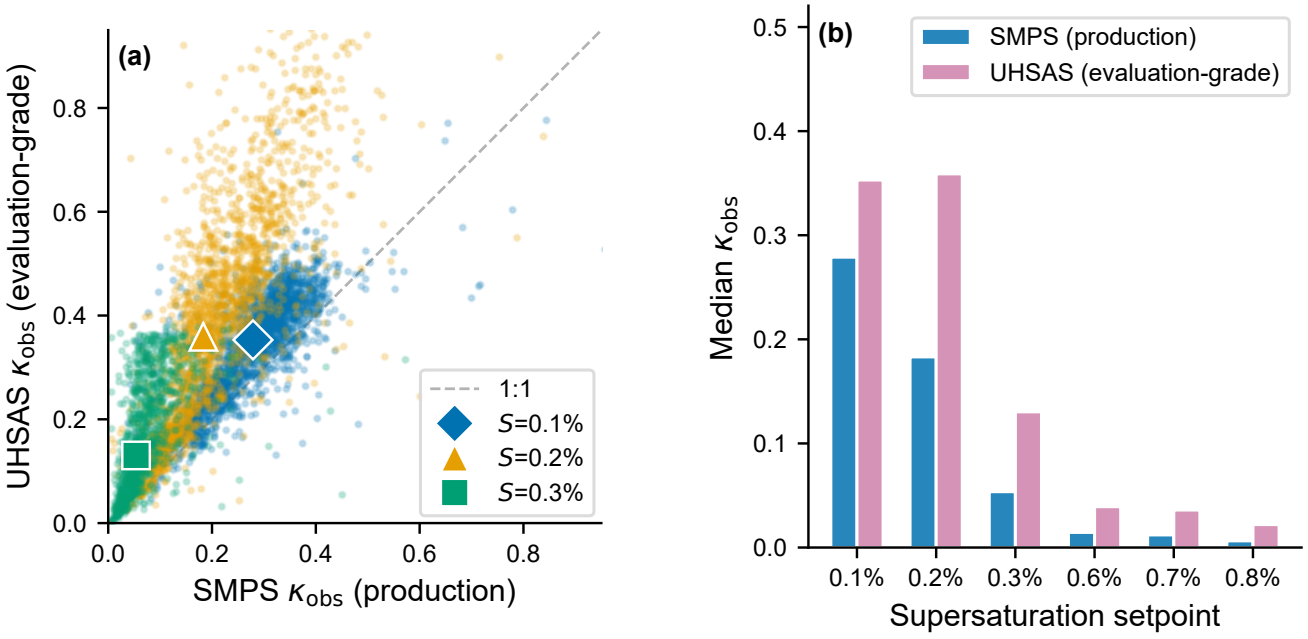

Figure 8. Time- and setpoint-matched κ_{obs} from the SMPS (production-grade) and UHSAS (evaluation-grade) CCN products on coincident air masses. At the 0.1% and 0.2% setpoints, the UHSAS product exceeds κ_{pred} and reverses the sign of the SMPS discrepancy. At higher setpoints, both products remain below κ_{pred}, although the UHSAS values are systematically higher. The product difference is consistent with sensitivity to the optical sizing undercount in Fig. 7, rather than a real hygroscopicity difference between instruments.

Table 8. Magnitude of the N_d divergence (%) between the two κ references, by updraft velocity and accumulation-mode number concentration. Because κ_{obs} is the biased quantity (Sect. 3.4), these are underestimates of N_d incurred by using the retrieved product.

w (m s^{-1})	clean ($N_{\mathrm{acc}} \approx 120$ cm^{-3})	typical ($N_{\mathrm{acc}} \approx 200$ cm^{-3})
0.1	12.1	9.4
0.2	15.9	14.9
0.3	16.1	14.4
0.5	20.3	14.8

https://doi.org/10.5194/egusphere-2026-5483
Preprint. Discussion started: 29 September 2026

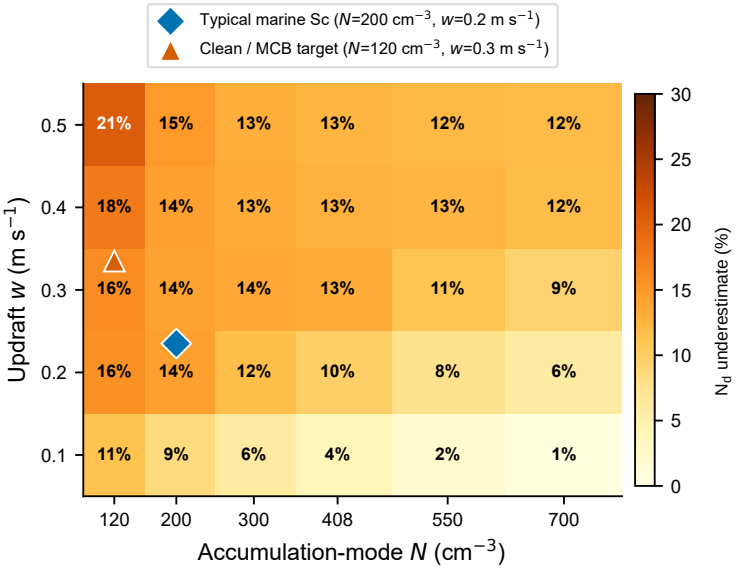

Figure 9. Magnitude of the N_d divergence (%) between the two κ references, as a function of updraft velocity w and accumulation-mode number concentration N_{acc}, under the Abdul-Razzak–Ghan activation closure (cf. Table 8). Because κ_{obs} is the biased quantity, these represent underestimates of N_d incurred by using the retrieved product.

$+24\%$, $+75\%$ and $+110\%$ at $S = 0.16$, 0.33 and 0.83%, respectively. These are far beyond the $\sim$5% typically reported for DMT CCN counters (Rose et al., 2008), and the required error would have to grow with nominal S rather than being fixed. A fixed multiplicative sizing or calibration error would also shift every setpoint by the same fractional amount. It could not produce a monotonic trend that steepens toward smaller particles. Composition bias is bounded in the same way. The ACSM measures non-refractory species only (Ng et al., 2011). Missing refractory sea salt ($\kappa_{\mathrm{NaCl}} \approx 1.1$) or a higher true organic hygroscopicity would each raise κ_{pred}, widening the discrepancy rather than closing it. Each setpoint fixes S and D_c together, so the closure comparison alone cannot distinguish genuine size-dependent hygroscopicity from a supersaturation-dependent retrieval response.

4.2 Implications for CCN closure studies

The UHSAS sizing bias and the mixing-state bias are the same mechanism acting through a different input. In both cases, an error in the number of particles the algorithm believes activated propagates, through the integration, into a D_c error, and from there nonlinearly into κ. Integration-based κ retrievals inherit any error in either the size distribution or the activation assumption, amplified by the cubic D_c-to-κ dependence.

This has practical consequences for any study using the product. At the three highest setpoints, a large fraction of quality-controlled records return $\kappa_{\mathrm{obs}} < 0.10$, a majority in two cases. These medians characterise a degraded retrieval rather than a

https://doi.org/10.5194/egusphere-2026-5483
Preprint. Discussion started: 29 September 2026

property of the aerosol. The primary result of this paper rests on the two lower setpoints, $S = 0.07\%$ and $S = 0.16\%$, where the corresponding fractions are only 1.4% and 17%. The activated-fraction saturation noted in Results is consistent with this. A population in which every particle above D_c activates would not produce a saturation near one half. A population in which only a hygroscopic subset activates would. Part of the shortfall is expected regardless, since the total includes particles too small to activate at any setpoint used here, and no attempt is made in this paper to partition the two contributions quantitatively.

Prior closure studies at ENA and comparable sites report agreement between retrieved and composition-predicted κ within calibration uncertainty (Zheng et al., 2018; Zawadowicz et al., 2021; Gallo et al., 2023). These studies used few supersaturation setpoints, and the trend documented here is not visible without enough setpoints to resolve it. Closure at any single setpoint, or across two or three, is consistent with the pattern found here rather than contradicting it.

Similar mixing-state-driven biases in CCN closure have been reported elsewhere. Ren et al. (2018) found N_{CCN} predictions in urban Beijing biased by -34% to $+16\%$ depending on the mixing-state assumption used. Ranjan et al. (2025) found that an internal-mixing assumption caused systematic CCN overprediction at a boreal forest site across supersaturations, resolved only by inferring size-resolved composition. Neither study documents the specific backward-integration mechanism identified here, but both support the broader point that mixing-state assumptions, not just size-distribution accuracy, are a recurring source of bias in CCN closure.

4.3 Comparison with Ai et al. (2026)

Ai et al. (2026) report a comparable supersaturation-dependent closure degradation at this same site from aircraft measurements and attribute it to size-dependent aerosol composition, on the grounds that CCN-inverted hygroscopicity there is nearly insensitive to bulk organic mass fraction while composition-based prediction assumes strong sensitivity.

The present results are consistent with that observation. The same qualitative pattern is reproduced here using five ground-based setpoints rather than two aircraft channels. Two channels cannot distinguish a genuine size-dependent hygroscopicity from a supersaturation-dependent retrieval response, since both predict the same monotonic decline with only two points to constrain it. Five setpoints, combined with an independent constraint on mixing state, allow that separation.

The HTDMA record analysed here reproduces the size-dependent hygroscopicity, accounting for about 20% of the observed decline. The insensitivity of CCN-inverted hygroscopicity to bulk organic fraction, which Ai et al. (2026) interpret as evidence that this size dependence explains the full trend, is also what the mechanism proposed here predicts. If the retrieved κ is set largely by the non-activating fraction of an externally mixed population rather than by the mean composition of the activating one, it should decouple from bulk composition regardless. The two interpretations make the same prediction on that diagnostic, so it does not discriminate between them.

The distinguishing evidence is the independent sub-saturated constraint and the forward simulation, neither of which was available in that study. It is therefore suggested that the attribution should be revisited where mixing-state measurements exist.

https://doi.org/10.5194/egusphere-2026-5483
Preprint. Discussion started: 29 September 2026

4.4 Representativeness

The closure statistics cover a single four-month period at one site, chosen by data availability rather than design, with the HTDMA comparison covering only the first 54 days of it. April–July represents the clean marine, sulfate-controlled regime that accounts for the majority of ENA observations (Wang et al., 2022). Figure 10 shows that S = 0.07% series tracks κ_{pred} through the campaign, while the S = 0.16% series sits persistently below it. The discrepancy is therefore sustained rather than driven by episodic events. No claim of generality to other seasons or sites is made.

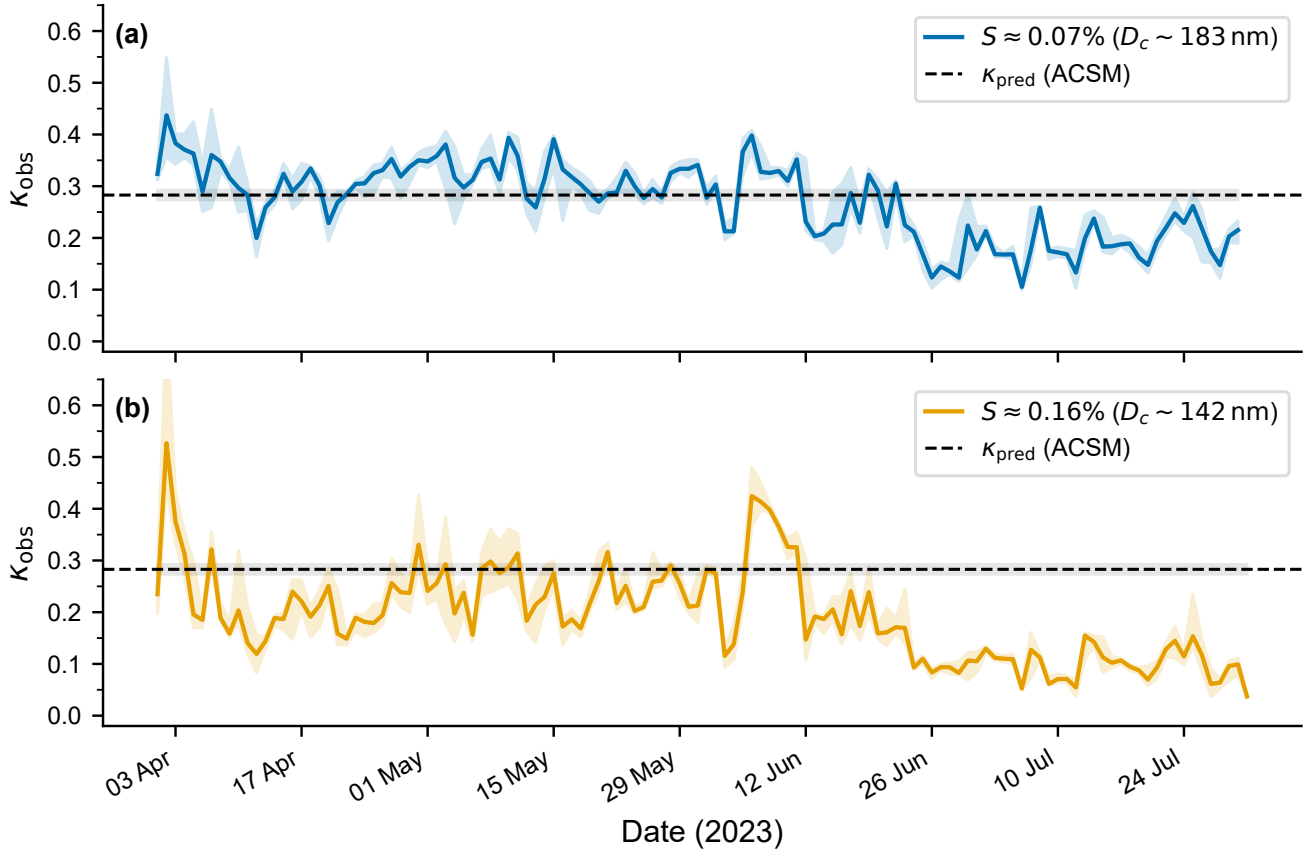

Figure 10. Time series of SMPS-derived κ_{obs} at the $S \approx 0.07\%$ ($D_c \approx 183$ nm) and $S \approx 0.16\%$ ($D_c \approx 142$ nm) setpoints, April–July 2023. The dashed line marks the campaign-median composition prediction, κ_{pred}. Coloured shading shows the daily interquartile range (25th–75th percentiles), while grey shading around κ_{pred} indicates ± 1 day-block bootstrap standard error.

Since ENA's organic fraction is seasonal (Wang et al., 2022), and the mixing state is what drives the bias, a winter campaign could plausibly show a different magnitude.

Methodological caveats attach to the mixing-state and forward-simulation results specifically. The HTDMA transfer function has finite width, so the dispersion values in Table 6 overstate the true external mixing. A full treatment would require inversion

https://doi.org/10.5194/egusphere-2026-5483
Preprint. Discussion started: 29 September 2026

of the instrument transfer function (Gysel et al., 2009). Two considerations limit the impact: comparisons across size are far more robust than absolute values, and instrumental broadening merges modes rather than creating them, so the multimodal fractions are a lower bound. The mode count is a smoothed-local-maximum proxy with a prominence threshold, not a formal test of multimodality. The forward simulation carries a 6% low bias by construction (Sect. 3.4), so the explained fractions in Table 7 may be slight over-estimates.

Finally, the simulation over-predicts the discrepancy at $S = 0.16\%$ (118%), the one setpoint where the mechanism does not simply fit. One candidate for that direction is the documented dichotomy between low sub-saturated hygroscopicity and high supersaturated CCN activity in primary marine organic aerosol (Ovadnevaite et al., 2011). Where such particles are present, the assumption that κ_{HTDMA} predicts activation would fail specifically toward under-predicting activation, consistent with the direction of the $S = 0.16\%$ discrepancy.

4.5 Consequences for cloud droplet number

The forward simulation identifies κ_{obs} as the biased quantity, not κ_{pred}. Because $S_c \propto \kappa^{-1/2}$, the lower retrieved κ implies a higher activation threshold, so using κ_{obs} in an activation calculation underestimates N_d relative to using κ_{pred}.

This underestimate is not a single fixed number. It differs depending on the accumulation-mode shape assumed. Holding the shape fixed at the campaign-median value gives the higher estimate, 13.9%. Resolving the shape hourly gives the lower estimate, 8.7%. The higher figure should be treated as an upper bound under that modelling choice.

The albedo consequence of this N_d bias, estimated in Results through the Twomey susceptibility, is first-order only. It holds liquid water path fixed and neglects the cloud adjustments that offset or amplify Twomey susceptibility in real stratocumulus (Ackerman et al., 2004; Wood, 2007). It is not developed further here.

5 Conclusions

A statistically significant, supersaturation-dependent discrepancy between CCN-retrieved and composition-predicted hygroscopicity has been documented at the ARM Eastern North Atlantic site, and its dominant cause has been identified. The discrepancy is monotonic across five setpoints, growing from $\delta\kappa = +0.004$ at $D_c \approx 183$ nm to $+0.219$ at $D_c \approx 67$ nm. It cannot be explained by sizing error, supersaturation calibration error, or composition bias, each of which is either of the wrong sign or requires an implausible magnitude.

An independent sub-saturated HTDMA record shows that genuine size-dependent hygroscopicity is present but accounts for only about 20 % of the retrieved decline. The same record shows substantial hygroscopic heterogeneity at every size sampled, with κ dispersion of 0.66–0.83 and 37–71 % of scans resolving multiple modes. The uniform-composition assumption underlying the retrieval is therefore not satisfied. Forward-simulating the retrieval using the measured hygroscopicity distributions reproduces the observed κ at every setpoint, accounting for 92–118 % of the discrepancy. The mechanism is that sufficiently large but insufficiently hygroscopic particles do not activate; consequently, the backward integration terminates at a diameter

https://doi.org/10.5194/egusphere-2026-5483
Preprint. Discussion started: 29 September 2026

larger than that implied by the uniform-composition assumption, biasing retrieved κ low through $\kappa \propto D_c^{-3}$. The bias increases as the non-activating fraction grows toward smaller critical diameters.

Previous closure studies at ENA and comparable marine sites have generally reported agreement between CCN-retrieved and composition-predicted hygroscopicity within measurement uncertainty, while recent observations at ENA have attributed supersaturation-dependent closure degradation primarily to size-dependent composition. The present results show that genuine size dependence is present but is too small to explain the observed trend, while mixing-state-dependent failure of the retrieval can reproduce its magnitude and supersaturation dependence.

The quantitative result is specific to the spring–summer period examined at ENA and will depend on aerosol size distribution and mixing state. The HTDMA comparison is restricted to the first 54 days of the campaign, and the forward simulation assumes that sub-saturated HTDMA-derived hygroscopicity can be used to represent supersaturated activation behaviour. Instrumental broadening of the HTDMA distributions and the finite size-bin resolution of the retrieval introduce additional uncertainty. These limitations affect the quantitative attribution but do not alter the observation that the aerosol population violates the uniformity assumption on which the retrieval is based.

When propagated through an Abdul-Razzak–Ghan activation calculation, use of the retrieved rather than reference κ produces an approximately 9–20 % underestimate in predicted cloud droplet number under the conditions examined. More generally, integration-based CCN retrievals can convert aerosol mixing-state heterogeneity into an apparent supersaturation dependence of hygroscopicity, which may subsequently propagate into estimates of aerosol activation and aerosol–cloud interactions. Supersaturation-dependent structure in retrieved κ should therefore be tested against independent constraints on aerosol mixing state before being interpreted as an atmospheric signal.

Code availability. Analysis code, including the mixing-state analysis and the forward simulation, is available at https://doi.org/10.5281/zenodo.21824109.

Data availability. All datasets are distributed by the ARM Data Center (https://adc.arm.gov) and are cited individually in the reference list: the SMPS-CCN κ product (Kulkarni and Uin, 2023), the UHSAS-CCN κ product (Kulkarni et al., 2023), the HTDMA record (Uin et al., 2021) and the ACSM composition record (Zawadowicz, 2023).

Author contributions. IB designed the study, performed the analysis, and wrote the manuscript. AC reviewed the manuscript.

Competing interests. The authors declare no competing interests.

https://doi.org/10.5194/egusphere-2026-5483
Preprint. Discussion started: 29 September 2026

Acknowledgements. IB and AC acknowledge funding from the Engineering and Physical Sciences Research Council Centre for Doctoral Training in Aerosol Science (grant no. EP/S023593/1) and the University of Cambridge Centre for Climate Repair. Preliminary investigation was carried out at the Cambridge Earthlab workshop with the aid of AC and Francesco Muschitiello. The authors thank Jurgita Ovadnevaite for helpful discussions on marine aerosol hygroscopicity and differences between subsaturated and supersaturated water uptake. The authors thank Edward Gryspeerdt for his feedback on the interpretation and manuscript.

https://doi.org/10.5194/egusphere-2026-5483
Preprint. Discussion started: 29 September 2026

References

Abdul-Razzak, H. and Ghan, S. J.: A parameterization of aerosol activation, 2. Multiple aerosol types, Journal of Geophysical Research, 105, 6837–6844, https://doi.org/10.1029/1999JD901161, 2000.

Ackerman, A. S., Kirkpatrick, M. P., Stevens, D. E., and Toon, O. B.: The impact of humidity above stratiform clouds on indirect aerosol climate forcing, Nature, 432, 1014–1017, https://doi.org/10.1038/nature03174, 2004.

Ai, G., Tang, S., Wang, H., Mei, F., and Wang, M.: Dependence of CCN closure relationship with organic fraction from two airborne field campaigns over mid-latitude land and ocean, Atmospheric Chemistry and Physics, 26, 7967–7984, https://doi.org/10.5194/acp-26-7967-2026, 2026.

Bougiatioti, A., Nenes, A., Fountoukis, C., Kalivitis, N., Pandis, S. N., and Mihalopoulos, N.: Size-resolved CCN distributions and activation kinetics of aged continental and marine aerosol, Atmospheric Chemistry and Physics, 11, 8791–8808, https://doi.org/10.5194/acp-11-8791-2011, 2011.

Cai, Y., Montague, D. C., Mooiweer-Bryan, W., and Deshler, T.: Performance characteristics of the ultra high sensitivity aerosol spectrometer for particles between 55 and 800 nm: Laboratory and field studies, Journal of Aerosol Science, 39, 759–769, https://doi.org/10.1016/j.jaerosci.2008.04.007, 2008.

Cerully, K. M., Raatikainen, T., Lance, S., Tkacik, D., Tiitta, P., Petäjä, T., Ehn, M., Kulmala, M., Worsnop, D. R., Laaksonen, A., Smith, J. N., and Nenes, A.: Aerosol hygroscopicity and CCN activation kinetics in a boreal forest environment during the 2007 EUCAARI campaign, Atmospheric Chemistry and Physics, 11, 12 369–12 386, https://doi.org/10.5194/acp-11-12369-2011, 2011.

Dusek, U., Frank, G., Hildebrandt, L., Curtius, J., Schneider, J., Walter, S., Chand, D., Drewnick, F., Hings, S., Jung, D., Borrmann, S., and Andreae, M. O.: Size Matters More Than Chemistry for Cloud-Nucleating Ability of Aerosol Particles, Science, 312, 1375–1378, https://doi.org/10.1126/science.1125261, 2006.

Gallo, F., Uin, J., Sanchez, K. J., Moore, R. H., Wang, J., Wood, R., Mei, F., Flynn, C., Springston, S., Azevedo, E. B., Kuang, C., and Aiken, A. C.: Long-range transported continental aerosol in the eastern North Atlantic: three multiday event regimes influence cloud condensation nuclei, Atmospheric Chemistry and Physics, 23, 4221–4246, https://doi.org/10.5194/acp-23-4221-2023, 2023.

Gysel, M., McFiggans, G. B., and Coe, H.: Inversion of Tandem Differential Mobility Analyser (TDMA) Measurements, Journal of Aerosol Science, 40, 134–151, https://doi.org/10.1016/j.jaerosci.2008.07.013, 2009.

Köhler, H.: The nucleus in and the growth of hygroscopic droplets, Transactions of the Faraday Society, 32, 1152–1161, https://doi.org/10.1039/TF9363201152, 1936.

Kulkarni, G. and Uin, J.: Cloud Condensation Nuclei (CCN) Counter and Scanning Mobility Particle Sizer (SMPS) Derived Hygroscopicity Parameter Kappa (CCNSMPSKAPPA), https://doi.org/10.5439/1729907, aRM Data Center, Eastern North Atlantic (ENA) site, 2023.

Kulkarni, G., Levin, M. S., and Shilling, J.: Cloud Condensation Nuclei Hygroscopicity Value-Added Product Report, Tech. Rep. DOE/SC-ARM-TR-272, U.S. Department of Energy, Atmospheric Radiation Measurement user facility, Richland, WA, https://doi.org/10.2172/1818210, 2021.

Kulkarni, G., Levin, M., and Shilling, J.: AOS: CCN Counter and UHSAS derived hygroscopicity parameter kappa, https://doi.org/10.5439/1984049, atmospheric Radiation Measurement (ARM) User Facility, Eastern North Atlantic (ENA) site, datastream enaaosccnuhsaskappaC1.c1, evaluation-grade product, 2023.

https://doi.org/10.5194/egusphere-2026-5483
Preprint. Discussion started: 29 September 2026

Kupc, A., Williamson, C., Wagner, N. L., Richardson, M. S., and Brock, C.: Modification, calibration, and performance of the Ultra-High Sensitivity Aerosol Spectrometer for particle size distribution and volatility measurements during the Atmospheric Tomography Mission (ATom) airborne campaign, Atmospheric Measurement Techniques, 11, 369–383, https://doi.org/10.5194/amt-11-369-2018, 2018.

Mather, J. H. and Voyles, J. W.: The ARM Climate Research Facility: a review of structure and capabilities, Bulletin of the American Meteorological Society, 94, 377–392, https://doi.org/10.1175/BAMS-D-11-00218.1, 2013.

Middlebrook, A. M., Bahreini, R., Jimenez, J. L., and Canagaratna, M. R.: Evaluation of Composition-Dependent Collection Efficiencies for the Aerodyne Aerosol Mass Spectrometer using Field Data, Aerosol Science and Technology, 46, 258–271, https://doi.org/10.1080/02786826.2011.620041, 2012.

Ng, N. L., Herndon, S. C., Trimborn, A., Canagaratna, M. R., Croteau, P. L., Onasch, T. B., Sueper, D., Worsnop, D. R., Zhang, Q., Sun, Y. L., and Jayne, J. T.: An Aerosol Chemical Speciation Monitor (ACSM) for Routine Monitoring of the Composition and Mass Concentrations of Ambient Aerosol, Aerosol Science and Technology, 45, 780–794, https://doi.org/10.1080/02786826.2011.560211, 2011.

Ovadnevaite, J., Ceburnis, D., Martucci, G., Bialek, J., Monahan, C., Rinaldi, M., Facchini, M. C., Berresheim, H., Worsnop, D. R., and O'Dowd, C.: Primary marine organic aerosol: A dichotomy of low hygroscopicity and high CCN activity, Geophysical Research Letters, 38, https://doi.org/10.1029/2011GL048869, 2011.

Petters, M. D. and Kreidenweis, S. M.: A single parameter representation of hygroscopic growth and cloud condensation nucleus activity, Atmospheric Chemistry and Physics, 7, 1961–1971, https://doi.org/10.5194/acp-7-1961-2007, 2007.

Platnick, S. and Twomey, S.: Determining the susceptibility of cloud albedo to changes in droplet concentration with the Advanced Very High Resolution Radiometer, Journal of Applied Meteorology, 33, 334–347, https://doi.org/10.1175/1520-0450(1994)033<0334:DTSOCA>2.0.CO;2, 1994.

Ranjan, R., Dewey, M., Heikkinen, L., Ahonen, L. R., Luoma, K., Bowen, P., Petäjä, T., Ekman, A. M. L., Partridge, D. G., and Riipinen, I.: Optimizing CCN predictions through inferred modal aerosol composition – a boreal forest case study, Atmospheric Chemistry and Physics, 25, 17 275–17 300, https://doi.org/10.5194/acp-25-17275-2025, 2025.

Ren, J., Zhang, F., Wang, Y., Collins, D., Fan, X., Jin, X., Xu, W., Sun, Y., Cribb, M., and Li, Z.: Using different assumptions of aerosol mixing state and chemical composition to predict CCN concentrations based on field measurements in urban Beijing, Atmospheric Chemistry and Physics, 18, 6907–6921, https://doi.org/10.5194/acp-18-6907-2018, 2018.

Rose, D., Gunthe, S. S., Mikhailov, E., Frank, G. P., Andreae, M. O., and Pöschl, U.: Calibration and measurement uncertainties of a continuous-flow cloud condensation nuclei counter (DMT-CCNC), Atmospheric Chemistry and Physics, 8, 1153–1179, https://doi.org/10.5194/acp-8-1153-2008, 2008.

Shilling, J. E. and Levin, M.: Aerosol Chemical Speciation Monitor (ACSM) Composition-Dependent Collection Efficiency (CDCE) Value-Added Product Report, Tech. Rep. DOE/SC-ARM-TR-271, Pacific Northwest National Laboratory, Richland, WA, https://doi.org/10.2172/1813010, 2021.

Swietlicki, E., Hansson, H.-C., Hämeri, K., Svenningsson, B., Massling, A., McFiggans, G., McMurry, P. H., Petäjä, T., Tunved, P., Gysel, M., Topping, D., Weingartner, E., Baltensperger, U., Rissler, J., Wiedensohler, A., and Kulmala, M.: Hygroscopic Properties of Sub-Micrometer Atmospheric Aerosol Particles Measured with H-TDMA Instruments in Various Environments – A Review, Tellus B: Chemical and Physical Meteorology, 60, 432–469, https://doi.org/10.1111/j.1600-0889.2008.00350.x, 2008.

Uin, J., Aiken, A. C., Dubey, M. K., Kuang, C., Pekour, M., Salwen, C., Sedlacek, A. J., Senum, G., Smith, S., Wang, J., Watson, T. B., and Springston, S. R.: Atmospheric Radiation Measurement (ARM) Aerosol Observing Systems (AOS) for Surface-

https://doi.org/10.5194/egusphere-2026-5483
Preprint. Discussion started: 29 September 2026

Based In-Situ Atmospheric Aerosol and Trace Gas Measurements, Journal of Atmospheric and Oceanic Technology, 36, 2429–2447, https://doi.org/10.1175/JTECH-D-19-0077.1, 2019.

Uin, J., Cromwell, E., Hayes, C., and Salwen, C.: Humidified Tandem Differential Mobility Analyser (HTDMA) (aoshtdma.b1), https://doi.org/10.5439/1776643, aRM Data Center, Eastern North Atlantic (ENA) site, 2021.

Wang, J., Wood, R., Jensen, M. P., Chiu, J. C., Liu, Y., Lamer, K., Desai, N., Giangrande, S. E., Knopf, D. A., Kollias, P., Laskin, A., Liu, X., Lu, C., Mechem, D., Mei, F., Starzec, M., Tomlinson, J., Wang, Y., and Zhang, Z.: Aerosol and cloud experiments in the Eastern North Atlantic (ACE-ENA), Bulletin of the American Meteorological Society, 103, E619–E641, https://doi.org/10.1175/BAMS-D-19-0220.1, 2022.

Wiedensohler, A., Birmili, W., Nowak, A., Sonntag, A., Weinhold, K., Merkel, M., Wehner, B., Tuch, T., Pfeifer, S., Fiebig, M., Fjäraa, A. M., Asmi, E., Sellegri, K., Depuy, R., Venzac, H., Villani, P., Laj, P., Aalto, P., Ogren, J. A., Swietlicki, E., Williams, P., Roldin, P., Quincey, P., Hüglin, C., Fierz-Schmidhauser, R., Gysel, M., Weingartner, E., Riccobono, F., Santos, S., Grüning, C., and Faloon, K.: Mobility particle size spectrometers: harmonization of technical standards and data structure to facilitate high quality long-term observations of atmospheric particle number size distributions, Atmospheric Measurement Techniques, 5, 657–685, https://doi.org/10.5194/amt-5-657-2012, 2012.

Wood, R.: Cancellation of Aerosol Indirect Effects in Marine Stratocumulus through Cloud Thinning, Journal of the Atmospheric Sciences, 64, 2657–2669, https://doi.org/10.1175/JAS3942.1, 2007.

Xu, W., Fossum, K. N., Ovadnevaite, J., Lin, C., Huang, R.-J., O'Dowd, C., and Ceburnis, D.: The impact of aerosol size-dependent hygroscopicity and mixing state on the cloud condensation nuclei potential over the north-east Atlantic, Atmospheric Chemistry and Physics, 21, 8655–8675, https://doi.org/10.5194/acp-21-8655-2021, 2021.

Zawadowicz, M.: Aerosol Chemical Speciation Monitor (AOSACSM), https://doi.org/10.5439/1558768, aRM Data Center, Eastern North Atlantic (ENA) site, 2023.

Zawadowicz, M. A., Suski, K., Liu, J., Pekour, M., Fast, J., Mei, F., Sedlacek, A. J., Springston, S., Wang, Y., Zaveri, R. A., Wood, R., Wang, J., and Shilling, J. E.: Aircraft measurements of aerosol and trace gas chemistry in the eastern North Atlantic, Atmospheric Chemistry and Physics, 21, 7983–8002, https://doi.org/10.5194/acp-21-7983-2021, 2021.

Zheng, G., Wang, Y., Aiken, A. C., Gallo, F., Jensen, M. P., Kollias, P., Kuang, C., Luke, E., Springston, S., Uin, J., Wood, R., and Wang, J.: Marine boundary layer aerosol in the eastern North Atlantic: seasonal variations and key controlling processes, Atmospheric Chemistry and Physics, 18, 17 615–17 635, https://doi.org/10.5194/acp-18-17615-2018, 2018.